J. Fluid Mech. (2014), *vol.* 757, *pp.* 381–402.
doi:10.1017/jfm.2014.509

Parametric subharmonic instability of internal waves: locally confined beams versus monochromatic wavetrains

Hussain H. Karimi[1] **and T. R. Akylas**[1,†]

[1]Department of Mechanical Engineering, Massachusetts Institute of Technology, Cambridge, MA 02139, USA

(Received 17 April 2014; revised 9 July 2014; accepted 30 August 2014; first published online 17 September 2014)

Internal gravity wavetrains in continuously stratified fluids are generally unstable as a result of resonant triad interactions which, in the inviscid limit, amplify short-scale perturbations with frequency equal to one half of that of the underlying wave. This so-called parametric subharmonic instability (PSI) has been studied extensively for spatially and temporally monochromatic waves. Here, an asymptotic analysis of PSI for time-harmonic plane waves with locally confined spatial profile is made, in an effort to understand how such wave beams differ, in regard to PSI, from monochromatic plane waves. The discussion centres upon a system of coupled evolution equations that govern the interaction of a small-amplitude wave beam with short-scale subharmonic wavepackets in a nearly inviscid uniformly stratified Boussinesq fluid. For beams with general localized profile, it is found that triad interactions are not strong enough to bring about instability in the limited time that subharmonic perturbations overlap with the beam. On the other hand, for quasi-monochromatic wave beams whose profile comprises a sinusoidal carrier modulated by a locally confined envelope, PSI is possible if the beam is wide enough. In this instance, a stability criterion is proposed which, under given flow conditions, provides the minimum number of carrier wavelengths a beam of small amplitude must comprise for instability to arise.

Key words: geophysical and geological flows, instability, internal waves

1. Introduction

There is an extensive literature on the stability of internal gravity waves in continuously stratified fluids with applications to various geophysical processes. Most stability analyses assume uniform stratification in the Boussinesq approximation. Under these flow conditions, the background buoyancy frequency is constant and, moreover, sinusoidal plane waves are not only linear solutions, but also exact nonlinear states of the governing equations in the inviscid limit. A uniformly stratified Boussinesq fluid thus affords a convenient setting for examining the stability of periodic wavetrains of arbitrary amplitude.

This problem has been addressed by numerous investigations (see Staquet & Sommeria 2002 for a review), and it is now well established that instability of

† Email address for correspondence: trakylas@mit.edu

small-amplitude internal waves is instigated by resonant nonlinear wave interactions (see Phillips 1981 for a review). Specifically, ignoring dissipation, weakly nonlinear sinusoidal internal waves are unstable to infinitesimal perturbations that form resonant triads with the underlying wavetrain. In addition, the unstable perturbations singled out by triad interactions are of short wavelength and have frequency equal to one half of that of the primary wave. This so-called parametric subharmonic instability (PSI) has received a great deal of attention as a potential mechanism for transferring energy from large-scale internal waves to small-scale mixing in oceans (see, for example, Hibiya, Nagasawa & Niwa 2002; Koudella & Staquet 2006; MacKinnon *et al.* 2013).

However, as argued by Sutherland (2013), the PSI found in stability analyses of spatially and temporally monochromatic internal wavetrains may not be entirely relevant to ocean internal waves. In fact, an inviscid, uniformly stratified Boussinesq fluid supports time-harmonic plane waves with general spatial profile which propagate along a direction to the vertical determined by the wave frequency. These disturbances, often referred to as wave beams, are fundamental to internal wave motion and, like sinusoidal wavetrains, happen to be exact nonlinear states of the governing equations (McEwan 1973; Tabaei & Akylas 2003).

In oceans, wave beams with locally confined profile arise from the interaction of the barotropic tide with sea-floor topography, as demonstrated by theoretical and numerical models (Bell 1975; Khatiwala 2003; Lamb 2004), laboratory experiments (Gostiaux & Dauxois 2007; Zhang, King & Swinney 2007; Peacock, Echeverri & Balmforth 2008) and field observations (Lien & Gregg 2001; Cole *et al.* 2009; Johnston *et al.* 2011). In contrast to sinusoidal wavetrains which are generally prone to PSI, however, no evidence of PSI in wave beams is reported in these studies. Moreover, the same is true for internal wave beams generated in several laboratory experiments by oscillating a body in a stratified fluid tank (see, for example, Mowbray & Rarity 1967; Sutherland *et al.* 1999; Sutherland & Linden 2002).

Yet, according to other recent studies, PSI can occur in internal wave beams under certain circumstances. Similar to earlier experiments, Clark & Sutherland (2010) used a vertically oscillating circular cylinder as wave source in a stratified fluid tank. However, the cylinder oscillations were of relatively large amplitude, resulting in beams with quasi-monochromatic profile which typically broke down as they propagated away from the forcing region. Clark & Sutherland (2010) indirectly linked this breakdown to PSI, a hypothesis also supported by numerical simulations. Furthermore, PSI was noted in an experimental–numerical study of a model internal tide (Pairaud *et al.* 2010), as well as in numerical simulations of the reflection of a localized nearly monochromatic wave beam from a horizontal surface (Zhou & Diamessis 2013). Finally, recent experiments (Bourget *et al.* 2013) have revealed that resonant triad interactions can bring about instability in a localized wave beam that comprises just three wavelengths of a sinusoidal wavetrain. However, the observed most unstable perturbations were not short-scale subharmonic disturbances because the dimensions in the experimental set-up, being orders of magnitude smaller than the typical ocean scales, amplified the effects of viscosity.

The present paper seeks to understand theoretically the conditions under which internal wave beams with locally confined profile may suffer PSI in a nearly inviscid, uniformly stratified Boussinesq fluid. In keeping with the salient features of PSI in this setting, the analysis focuses on subharmonic disturbances of short wavelength compared with the beam width, a picture also suggested by the numerical findings of Clark & Sutherland (2010). Such fine-scale wavepackets are modulated by and also interact nonlinearly with the underlying large-scale wave beam. To examine the

possibility of PSI as a result of this long–short wave interaction, coupled evolution equations are derived for the wavepacket envelopes and the beam profile, taking the beam and the perturbations to have small but finite amplitude.

The analysis brings out the fact that subharmonic wavepackets travel with their respective group velocities, so their interaction with a locally confined beam has finite duration; thus, PSI hinges upon whether, during this limited time, such perturbations can extract enough energy from the beam to overcome viscous dissipation. The decisive role, in regard to PSI, of the group velocity of short-scale subharmonic wavepackets riding on a large-scale internal wave, was first suggested by McEwan & Plumb (1977).

Based on the evolution equations derived here, it is argued that weakly nonlinear beams with general locally confined profile are stable to short-scale subharmonic perturbations, in stark contrast to the well-established PSI of weakly nonlinear monochromatic plane waves. The reason for this difference is that triad interactions, which are responsible for PSI, are not strong enough to cause instability during the limited time that the pertubations overlap with a beam of localized profile. An exception arises when the group velocity of subharmonic wavepackets happens to vanish or nearly so, a condition that can be satisfied when Coriolis effects are taken into account (Gerkema, Staquet & Bouruet-Aubertot 2006; Young, Tsang & Balmforth 2008). PSI of localized beams under this resonance is discussed in Karimi (2015).

On the other hand, triad interactions are capable of destabilizing quasi-monochromatic wave beams whose profile consists of a sinusoidal carrier wave modulated by a locally confined envelope. In this instance, the asymptotic theory reveals that PSI does occur if a beam is wide enough, and an explicit stability criterion is proposed in terms of the number of carrier wavelengths required for instability to arise. Although strictly valid for weakly nonlinear slowly modulated beams, the theoretical predictions seem consistent with the experiments and numerical simulations of Clark & Sutherland (2010), which involved finite-amplitude beams with just two carrier wavelengths.

2. Long–short wave interaction

Our analysis assumes two-dimensional disturbances in an incompressible, continuously stratified Boussinesq fluid with constant buoyancy frequency N_0. We shall work with dimensionless variables, employing $1/N_0$ as time scale and a characteristic length L_*, to be specified later, as length scale. With x being the horizontal and y the vertical coordinate pointing upwards, the steamfunction $\psi(x, y, t)$ for the velocity field $(\psi_y, -\psi_x)$, and the reduced density $\rho(x, y, t)$ are then governed by

$$\rho_t + \psi_x + \mathrm{J}(\rho, \psi) = 0, \tag{2.1}$$

$$\nabla^2\psi_t - \rho_x + \mathrm{J}(\nabla^2\psi, \psi) - \nu\nabla^4\psi = 0, \tag{2.2}$$

where $\mathrm{J}(a, b) = a_x b_y - a_y b_x$ stands for the Jacobian. The parameter

$$\nu = \frac{\nu_*}{N_0 L_*^2} \tag{2.3}$$

is an inverse Reynolds number, where ν_* denotes the fluid kinematic viscosity.

In the inviscid limit ($\nu = 0$), (2.1) and (2.2) support time-harmonic plane waves with general spatial profile. These so-called wave beams are manifestations of the anisotropy of internal gravity wave motion: according to the familiar dispersion relation

$$\omega = \sin\theta, \tag{2.4}$$

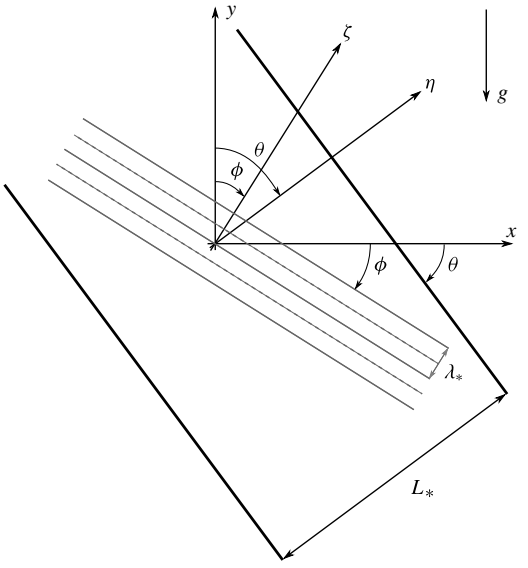

FIGURE 1. Geometry of long–short wave interaction. The underlying wave beam with general locally confined profile of characteristic width L_* has frequency ω and propagates at an angle θ to the horizontal such that $\omega = \sin\theta$. Subharmonic perturbations are short-crested ($\lambda_*/L_* \ll 1$) nearly monochromatic wavepackets with frequency close to $\omega/2$ that propagate at an angle ϕ to the horizontal, with $\sin\phi = (\sin\theta)/2$.

the frequency ω of a plane wave with sinusoidal profile depends on the inclination θ to the vertical, but not the magnitude, of the wavevector. Thus, by superposing sinusoidal plane waves with wavevectors of different magnitude but pointing in the same direction, it is possible to construct linear time-harmonic disturbances in the form of beams. Remarkably, this class of disturbances happen to be also nonlinear solutions of (2.1) and (2.2) for $\nu = 0$, irrespective of the beam profile (McEwan 1973; Tabaei & Akylas 2003). The dispersion relation (2.4) then links the frequency $0 < \omega < 1$ of a beam to its direction θ relative to the horizontal (figure 1).

The question of interest here is how wave beams with general locally confined profile differ from sinusoidal plane waves in regard to PSI. We shall address this issue via an asymptotic theory for weakly nonlinear beams under nearly inviscid flow conditions. Specifically, the non-dimensional beam amplitude ϵ is supposed to be small:

$$\epsilon = \frac{\psi_*}{N_0 L_*^2} \ll 1, \tag{2.5}$$

where ψ_* denotes the (dimensional) peak amplitude of the streamfunction and the length scale L_* is the characteristic width of the beam (figure 1). Also, viscous effects are assumed to be weak relative to nonlinear effects ($\nu/\epsilon \ll 1$; see (2.15) below), as is the case for spatial scales typical of ocean wave beams (Bourget *et al.* 2013).

Our discussion of PSI focuses on subharmonic perturbations in the form of fine-scale, nearly monochromatic wavepackets with frequency close to one half of the frequency $\omega = \sin\theta$ of the underlying beam. As discussed in § 1, this choice is motivated by earlier work on PSI of weakly nonlinear sinusoidal plane waves under nearly inviscid flow conditions (McEwan & Plumb 1977; Koudella & Staquet 2006), as well as laboratory experiments and numerical simulations of PSI of

quasi-monochromatic wave beams (Clark & Sutherland 2010). The dispersion relation (2.4), then, requires the wavepacket carrier wavevector $\boldsymbol{k}$ to be inclined to the vertical by ϕ, such that $\omega/2 = \sin\phi$, and we write

$$\boldsymbol{k}_{\pm} = \pm\frac{1}{\mu}\hat{\boldsymbol{e}}_{\zeta}. \tag{2.6}$$

Here $\hat{\boldsymbol{e}}_{\zeta}$ is a unit vector along $\zeta = x\sin\phi + y\cos\phi$ and μ is a small parameter, to express the fact that the perturbations are short-crested relative to the beam width:

$$\mu = \frac{\lambda_*}{2\pi L_*} \ll 1, \tag{2.7}$$

where λ_* denotes the (dimensional) carrier wavelength of the subharmonic wavepackets (figure 1).

Utilizing the presence of these two disparate lengthscales, we shall examine by asymptotic methods the possibility of the assumed perturbations extracting energy from the underlying wave beam, leading to instability. This long–short wave interaction is expected to take place on a time scale of $O(1/\mu)$, since, according to (2.4), the group velocities of wavepackets with carrier wavevectors (2.6) are $O(\mu)$:

$$\boldsymbol{c}_{g\pm} = \pm\mu(\cos^2\phi, -\sin\phi\cos\phi). \tag{2.8}$$

Thus, to study the evolution of the subharmonic perturbations due to their interaction with the wave beam, we define the 'slow' time

$$T = \mu t, \tag{2.9}$$

and introduce the following expansions for ψ and ρ:

$$\psi = \epsilon\{Q(\eta, T)\mathrm{e}^{-\mathrm{i}\omega t} + \text{c.c.}\} + \mu\delta\{(A(\eta, T)\mathrm{e}^{\mathrm{i}\zeta/\mu} + B(\eta, T)\mathrm{e}^{-\mathrm{i}\zeta/\mu})\mathrm{e}^{-\mathrm{i}\omega t/2} + \text{c.c.}\} + \cdots, \tag{2.10a}$$

$$\rho = \epsilon\{R(\eta, T)\mathrm{e}^{-\mathrm{i}\omega t} + \text{c.c.}\} + \delta\{(F(\eta, T)\mathrm{e}^{\mathrm{i}\zeta/\mu} + G(\eta, T)\mathrm{e}^{-\mathrm{i}\zeta/\mu})\mathrm{e}^{-\mathrm{i}\omega t/2} + \text{c.c.}\} + \cdots. \tag{2.10b}$$

The first curly bracket in expansions (2.10) represents the underlying wave beam with amplitude parameter ϵ; the second curly bracket represents the superposed subharmonic wavepackets with amplitude parameter $\delta \ll 1$ and carrier wavevectors given by (2.6). The beam profile amplitudes Q and R vary in the across-beam direction $\eta = x\sin\theta + y\cos\theta$, which is also the spatial modulation variable of the wavepacket envelopes A, B, F and G. In stability studies based on the so-called 'pump wave' approximation, the perturbation amplitude parameter δ is assumed to be infinitesimal ($\delta \ll \epsilon$), and the beam profile is frozen in time. As unstable perturbations grow at the expense of the underlying beam, however, eventually some feedback is anticipated, so Q and R are allowed to evolve with T in (2.10). The magnitude of δ relative to ϵ for such full coupling to take place is determined below (see (2.16)); ϵ and δ, as well as ν and μ introduced earlier, are treated as independent small parameters at this stage.

Upon substituting expansions (2.10) into the governing equations (2.1) and (2.2), we collect terms proportional to $\exp(-\mathrm{i}\omega t)$ and $\exp(\pm\mathrm{i}\zeta/\mu)\exp(-\mathrm{i}\omega t/2)$. This results in six coupled equations for the beam amplitudes Q and R and the subharmonic wavepacket envelopes A, B, F and G. After consistent elimination of R, F and G, the

following system of equations for Q, A and B is obtained:

$$\mu Q_T - \frac{\mathrm{i}}{2\omega}\mu^2 Q_{TT} + 2\frac{\delta^2}{\epsilon}\sin\chi\cos^2\frac{1}{2}\chi AB - \frac{\nu}{2}Q_{\eta\eta} = O(\mu^3, \mu\delta^2/\epsilon), \tag{2.11}$$

$$\mu\left(A_T + cA_\eta\right) - \frac{\mathrm{i}}{2}\mu^2 c' A_{\eta\eta} + \frac{1}{2}\frac{\nu}{\mu^2}A - \mathrm{i}\frac{\epsilon^2}{\mu^2}\frac{\sin^2\chi}{\omega}\left|Q_\eta\right|^2 A + \epsilon\sin\chi\left\{\frac{3}{2}Q_{\eta\eta}B^* + \frac{2}{\omega}Q_\eta B_T^* + \frac{1}{\omega}Q_{\eta T}B^*\right\} = O(\epsilon\mu, \mu^3, \delta^2, \epsilon^2/\mu), \tag{2.12a}$$

$$\mu\left(B_T - cB_\eta\right) - \frac{\mathrm{i}}{2}\mu^2 c' B_{\eta\eta} + \frac{1}{2}\frac{\nu}{\mu^2}B - \mathrm{i}\frac{\epsilon^2}{\mu^2}\frac{\sin^2\chi}{\omega}\left|Q_\eta\right|^2 B + \epsilon\sin\chi\left\{\frac{3}{2}Q_{\eta\eta}A^* - \frac{2}{\omega}Q_\eta A_T^* - \frac{1}{\omega}Q_{\eta T}A^*\right\} = O(\epsilon\mu, \mu^3, \delta^2, \epsilon^2/\mu), \tag{2.12b}$$

where

$$c = \frac{\omega}{2}(2 - \cos\chi), \quad c' = \frac{\omega}{2}(3\cos^2\chi - 4\cos\chi - 1). \tag{2.13a,b}$$

Here, $\chi = \theta - \phi$ and * denotes complex conjugate. Details of the derivation of this system are given in appendix A.

Focusing on (2.12) and recalling that $T = \mu t$, the leading-order terms indicate that the envelopes A and B of the subharmonic wavepackets travel across the beam with speed $\pm\mu c = \boldsymbol{c}_{g_\pm}\cdot\hat{\boldsymbol{e}}_\eta$, the projection of the respective group velocity (2.8) on the modulation direction η, where $\hat{\boldsymbol{e}}_\eta$ is a unit vector along η. The higher-order terms in (2.12) account for the $O(\mu^2)$ effects of dispersion, the $O(\nu/\mu^2)$ effects of viscous dissipation and the nonlinear effects due to the coupling with the underlying beam. The latter comprise $O(\epsilon^2/\mu^2)$ cubic terms, which can only affect the phases of the complex envelopes A and B and may be interpreted as nonlinear refraction terms, as well as $O(\epsilon)$ quadratic interaction terms which may give rise to energy exchange with the beam.

Based on (2.12) and (2.13), we now determine the proper balance between the small parameters ϵ, μ, ν and δ so that nonlinear, dispersive and viscous effects partake equally in the coupled evolution of the subharmonic perturbations with the underlying beam. From (2.12), the $O(\mu^2)$ dispersive terms are as important as the $O(\epsilon)$ quadratic interaction and the $O(\epsilon^2/\mu^2)$ nonlinear refraction terms, if $\mu\sim\epsilon^{1/2}$. Thus, we put

$$\mu = \frac{\epsilon^{1/2}}{\kappa}, \tag{2.14}$$

where $\kappa = O(1)$ is a normalized carrier wavenumber of the subharmonic wavepackets. In view of (2.14), the scaling

$$\nu = 2\alpha\epsilon^2, \tag{2.15}$$

where $\alpha = O(1)$, then brings the effects of viscous dissipation to the same level as those of dispersion and nonlinearity. Finally, returning to (2.11), for the beam amplitude Q to evolve on the same time scale as the wavepacket envelopes A and B, we set

$$\delta = \epsilon. \tag{2.16}$$

Hence, full nonlinear coupling occurs when the subharmonic perturbations reach an amplitude comparable with that of the underlying beam. Also, from (2.14)–(2.16), it is

now clear that the $O(\nu)$ viscous term in (2.11) is relatively small in comparison with the quadratic interaction term; naturally, viscous dissipation predominantly affects the perturbations, as they are of fine scale relative to the beam.

Upon implementing (2.14)–(2.16), (2.11) and (2.12), correct to $O(\epsilon^{1/2})$, become

$$Q_{T'} + 2\epsilon^{1/2} \sin\chi \cos^2\left(\tfrac{1}{2}\chi\right) AB = 0, \tag{2.17}$$

$$A_{T'} + \frac{c}{\kappa} A_\eta - \frac{\mathrm{i}}{2}\epsilon^{1/2}\frac{c'}{\kappa^2}A_{\eta\eta} + \epsilon^{1/2}\alpha\kappa^2 A - \mathrm{i}\epsilon^{1/2}\kappa^2\frac{\sin^2\chi}{\omega}\left|Q_\eta\right|^2 A + \epsilon^{1/2}\sin\chi\left\{\frac{3}{2}Q_{\eta\eta}B^* + 2\frac{c}{\omega}Q_\eta B^*_\eta\right\} = 0, \tag{2.18a}$$

$$B_{T'} - \frac{c}{\kappa} B_\eta - \frac{\mathrm{i}}{2}\epsilon^{1/2}\frac{c'}{\kappa^2}B_{\eta\eta} + \epsilon^{1/2}\alpha\kappa^2 B - \mathrm{i}\epsilon^{1/2}\kappa^2\frac{\sin^2\chi}{\omega}\left|Q_\eta\right|^2 B + \epsilon^{1/2}\sin\chi\left\{\frac{3}{2}Q_{\eta\eta}A^* + 2\frac{c}{\omega}Q_\eta A^*_\eta\right\} = 0, \tag{2.18b}$$

where

$$T' = \epsilon^{1/2} t = \kappa T. \tag{2.19}$$

According to the evolution equations (2.18), subharmonic perturbation wavepackets are expected to travel across a beam of $O(1)$ width virtually intact. As noted earlier, of the dispersive, nonlinear and viscous effects in (2.18), only the quadratic interaction terms are potentially destabilizing. These terms, however, being $O(\epsilon^{1/2})$, are small relative to the propagation terms associated with the wavepacket group velocities, and cannot bring about instability in the limited time that the perturbations are in contact with the underlying beam.

More specifically, in the pump-wave approximation where the beam profile $Q(\eta)$ does not evolve in time, the nonlinear refraction terms can be removed from (2.18) by letting

$$(A, B^*) \to (A, B^*)\exp\left\{\mathrm{i}\epsilon^{1/2}\frac{\kappa^3}{c\omega}\sin^2\chi\int^\eta \left|Q_\eta\right|^2 \mathrm{d}\eta\right\}. \tag{2.20}$$

As they modify only the phases of the wavepacket envelopes A and B, these terms have no impact on stability. Focusing now on the $O(\epsilon^{1/2})$ quadratic interaction terms in (2.18), to stand a chance of causing instability, they must be comparable with the $O(c/\kappa)$ propagation terms which control the duration of the interaction of the perturbations with the beam:

$$\frac{c}{\kappa} = O(\epsilon^{1/2}). \tag{2.21}$$

The above requirement could conceivably be satisfied by short-wavelength perturbations with $\kappa = O(\epsilon^{-1/2})$; in this limit, however, the phases of the wavepacket envelopes in (2.20) become $O(1/\epsilon)$ so they vary on the same scale as the carrier $\exp(\pm\mathrm{i}\zeta/\mu)$ in view of (2.10) and (2.14), violating the premises of the asymptotic theory. A feasible way to meet (2.21) is by taking $c = O(\epsilon^{1/2})$, which supposes that the wavepacket group velocities (2.8) nearly vanish; the perturbations then remain almost stationary and could extract significant energy from the underlying beam to cause instability. This resonant flow situation, although not possible here as is clear from (2.13), can arise when Coriolis effects are taken into account and is responsible, due to the Earth's rotation, for the instability of internal-tide beams to near-inertial subharmonic disturbances (Gerkema *et al.* 2006; Young *et al.* 2008). Detailed analysis of PSI under such resonant conditions is presented in Karimi (2015).

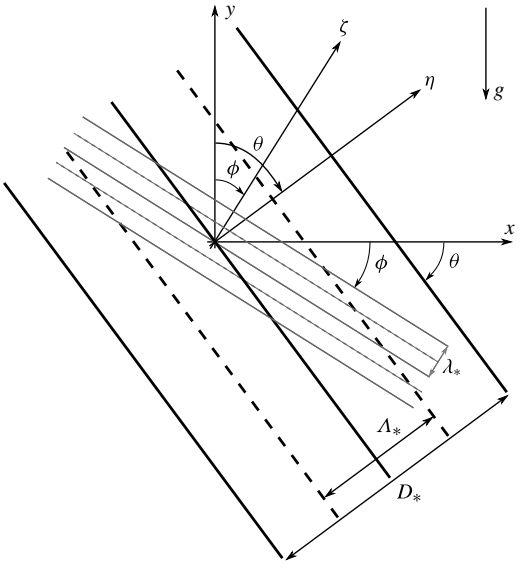

FIGURE 2. Schematic of interaction of nearly monochromatic wave beam of frequency $\omega = \sin\theta$ and non-dimensional amplitude $\epsilon \ll 1$ with subharmonic perturbations of frequency close to $\omega/2 = \sin\phi$. The beam profile comprises a sinusoidal carrier modulated by a slowly varying envelope, $\Lambda_*/D_* = O(\epsilon^{1/2})$, where Λ_* denotes the (dimensional) carrier wavelength and D_* the characteristic width of the envelope. The perturbations are short-scale wavepackets with (dimensional) carrier wavelength λ_*, such that $\lambda_*/\Lambda_* = O(\epsilon^{1/2})$.

Our conclusion that small-amplitude beams with general locally confined profile are stable to short-scale subharmonic perturbations may come as a surprise in view of the well-established PSI of weakly nonlinear sinusoidal plane waves. As noted in § 1, PSI of a monochromatic wave arises due to subharmonic disturbances that form resonant triads with the underlying wavetrain. For a localized beam with general profile of $O(1)$ width, however, this triad mechanism, while still present by virtue of the quadratic interaction terms in (2.18), cannot cause instability, as perturbations travel with their respective group velocities and triad interactions have relatively little time to act. To further clarify this essential difference between sinusoidal waves and localized beams, we now turn to a discussion of PSI for beams with profile in the form of a monochromatic carrier with $O(1)$ wavelength, modulated by a locally confined envelope.

3. Nearly monochromatic beam profile

Consider a uniform wave beam of frequency $\omega = \sin\theta$ with nearly monochromatic profile, involving a carrier modulated by a localized envelope (figure 2). Here it is convenient to choose as the characteristic length scale $L_* = \Lambda_*/2\pi$, where Λ_* denotes the (dimensional) carrier wavelength of the beam profile; thus, the beam carrier wavevector

$$\boldsymbol{k}_0 = \hat{\boldsymbol{e}}_\eta, \tag{3.1}$$

where $\hat{\boldsymbol{e}}_\eta$ is a unit vector in the cross-beam direction, as before. Also, the (dimensional) characteristic width of the beam envelope D_* satisfies $D_* \gg \Lambda_*$ (see (4.2) below for the precise scaling of D_* in terms of Λ_*).

The perturbations again are taken to be short-scale (relative to Λ_*) wavepackets with frequency close to $\omega/2 = \sin\phi$ (figure 2). Since PSI arises due to subharmonic disturbances that form resonant triads with the basic wavetrain, recalling (2.6) and (2.14), the wavepacket carrier wavevectors are chosen as

$$\boldsymbol{k}_\pm = \pm\frac{\kappa}{\epsilon^{1/2}}\hat{\boldsymbol{e}}_\zeta + \frac{1}{2}\boldsymbol{k}_0; \tag{3.2}$$

thus, $\boldsymbol{k}_+ + \boldsymbol{k}_- = \boldsymbol{k}_0$, as required for the members of a resonant triad. Upon substituting (3.2) in the dispersion relation (2.4) and making use of $\boldsymbol{c}_{g_\pm}\cdot\hat{\boldsymbol{e}}_\eta = \pm\epsilon^{1/2}c/\kappa$, with $\boldsymbol{c}_{g_\pm}$ and c as given in (2.8) and (2.13), respectively, we find

$$\omega_\pm = \frac{1}{2}\omega \pm \frac{1}{2}\frac{\epsilon^{1/2}}{\kappa}c + O(\epsilon); \tag{3.3}$$

hence, $\omega_+ + \omega_- = \omega + O(\epsilon)$. This confirms that $\boldsymbol{k}_+, \boldsymbol{k}_-$ and $\boldsymbol{k}_0$ form a resonant triad correct to $O(\epsilon^{1/2})$ and also suggests that the appropriate 'slow' time for the evolution of the subharmonic perturbation wavepackets is

$$\tau = \epsilon t. \tag{3.4}$$

Returning now to (2.17) and (2.18), we adapt these evolution equations to the problem at hand: the interaction of a nearly monochromatic beam of frequency ω and carrier wavevector $\boldsymbol{k}_0$ with two subharmonic wavepackets having carrier wavevectors (3.2) and frequencies (3.3). Specifically, combining (3.2) and (3.3) with (2.19), the appropriate expressions for the wavepacket envelopes $A(\eta, T')$ and $B(\eta, T')$ are

$$A = \exp\left\{\frac{\mathrm{i}}{2}\left(\eta - \frac{c}{\kappa}T'\right)\right\}a(\xi,\tau), \quad B = \exp\left\{\frac{\mathrm{i}}{2}\left(\eta + \frac{c}{\kappa}T'\right)\right\}b(\xi,\tau). \tag{3.5a,b}$$

Here, a and b are complex envelopes that evolve on the slow time τ defined in (3.4) and depend on the 'stretched' across-beam coordinate

$$\xi = \epsilon^{1/2}\eta, \tag{3.6}$$

such that spatial and temporal modulations are equally important. In addition, the profile amplitude $Q(\eta, T')$ of the nearly monochromatic wave beam with carrier wavevector (3.1) takes the form

$$Q = q(\xi,\tau)\mathrm{e}^{\mathrm{i}\eta}, \tag{3.7}$$

where q denotes the beam envelope, which also evolves on τ and depends on ξ; this ensures strong coupling with the two subharmonic wavepackets, as shown below.

Inserting (3.5) and (3.7) into (2.17) and (2.18), after some simplification making use of (2.13), we find that a, b and q are governed by

$$a_\tau + \frac{c}{\kappa}a_\xi + \frac{\mathrm{i}}{8}\frac{c'}{\kappa^2}a + \alpha\kappa^2 a - \mathrm{i}\frac{\kappa^2}{\omega}\sin^2\chi\,|q|^2 a - \sin\chi\cos^2\left(\frac{1}{2}\chi\right)qb^* = 0, \tag{3.8a}$$

$$b_\tau - \frac{c}{\kappa}b_\xi + \frac{\mathrm{i}}{8}\frac{c'}{\kappa^2}b + \alpha\kappa^2 b - \mathrm{i}\frac{\kappa^2}{\omega}\sin^2\chi\,|q|^2 b - \sin\chi\cos^2\left(\frac{1}{2}\chi\right)qa^* = 0, \tag{3.8b}$$

$$q_\tau + 2\sin\chi\cos^2\left(\tfrac{1}{2}\chi\right)ab = 0. \tag{3.9}$$

Finally, it is possible to remove the terms involving c' from (3.8),

$$a_\tau + \frac{c}{\kappa} a_\xi + \alpha\kappa^2 a - \mathrm{i}\frac{\kappa^2}{\omega} \sin^2\chi\, |q|^2\, a - \sin\chi \cos^2\left(\frac{1}{2}\chi\right) qb^* = 0, \tag{3.10a}$$

$$b_\tau - \frac{c}{\kappa} b_\xi + \alpha\kappa^2 b - \mathrm{i}\frac{\kappa^2}{\omega} \sin^2\chi\, |q|^2\, b - \sin\chi \cos^2\left(\frac{1}{2}\chi\right) qa^* = 0, \tag{3.10b}$$

by letting

$$a \to a \exp\left(-\mathrm{i}\frac{c'}{8c\kappa}\xi\right), \quad b \to b \exp\left(\mathrm{i}\frac{c'}{8c\kappa}\xi\right); \tag{3.11a,b}$$

this amounts to an $O(\epsilon^{1/2})$ shift of the carrier wavevectors $\boldsymbol{k}_\pm \to \boldsymbol{k}_\pm \mp (c'/8c\kappa)\epsilon^{1/2}\hat{\boldsymbol{e}}_\eta$ in (3.2).

As a result of the scalings chosen above, no small parameter appears explicitly in the evolution equations (3.9) and (3.10). In this 'distinguished limit', the effects that control the interaction of the subharmonic wavepacket envelopes a and b with the beam envelope q, are equally important. Specifically, according to (3.10), the transport of a and b with their respective group velocities is balanced by viscous and nonlinear effects, while at the same time q is evolving in response to its nonlinear coupling with a and b, as described by (3.9).

The system of equations (3.9) and (3.10) forms the basis for the discussion of PSI of wave beams in the remainder of the paper.

4. Stability analysis

A uniform beam corresponds to the steady-state solution

$$q = \overline{q}(\xi), \tag{4.1}$$

with $a = b = 0$, of (3.9) and (3.10). The linear stability of this state is examined by assuming that perturbations are small compared with the underlying beam ($|a|, |b| \ll |q|$). It then follows from (3.9) that q is frozen in time (pump-wave approximation), so a, b are governed by (3.10) with $q = \overline{q}(\xi)$.

To bring out the effect of the finite extent of a beam, we let $\xi \to \xi/D$ and take $\overline{q}(\xi)$ to have fixed $O(1)$ width. Here, D is the scaled width of the beam envelope in terms of the beam carrier wavelength,

$$D = 2\pi\frac{D_*}{\Lambda_*}\epsilon^{1/2} = 2\pi N\epsilon^{1/2}, \tag{4.2}$$

and $N = D_*/\Lambda_*$ measures the number of carrier wavelengths contained in the beam (see figure 2). It is also convenient to factor out the refraction terms in (3.10), which have no impact on stability, via a substitution analogous to (2.20)

$$(a, b^*) \to (a, b^*) \exp\left\{\mathrm{i}\frac{D\kappa^3}{\omega c} \sin^2\chi \int^\xi |\overline{q}|^2\, \mathrm{d}\xi'\right\}. \tag{4.3}$$

Thus, a and b satisfy the reduced system

$$a_\tau + \frac{c}{D\kappa} a_\xi + \alpha\kappa^2 a - \gamma\overline{q}b^* = 0, \tag{4.4a}$$

$$b_\tau - \frac{c}{D\kappa} b_\xi + \alpha\kappa^2 b - \gamma\overline{q}a^* = 0, \tag{4.4b}$$

with

$$\gamma = \sin\chi \cos^2\left(\tfrac{1}{2}\chi\right). \tag{4.5}$$

4.1. *Sinusoidal wavetrain*

From (4.4), it is easy to recover the well-known PSI of weakly nonlinear sinusoidal wavetrains by letting $D \to \infty$ and setting $\overline{q} = 1/2$; the peak amplitude of the wave streamfunction is thus normalized to ϵ, according to (2.10*a*) and (3.7). Normal-mode solutions, $(a, b^*) \propto \exp(\lambda\tau)$, of (4.4) then satisfy

$$\left(\lambda + \alpha\kappa^2\right)^2 = \tfrac{1}{4}\gamma^2, \tag{4.6}$$

and the disturbance growth rate is

$$\lambda = \tfrac{1}{2}\gamma - \alpha\kappa^2. \tag{4.7}$$

Using (4.5) and recalling that $\chi = \theta - \phi$ with $\sin\theta = 2\sin\phi$, it can be verified, after some trigonometry, that (4.7) in the inviscid limit ($\alpha = 0$) agrees with the growth rate of inviscid PSI quoted in equation (10) of Koudella & Staquet (2006).

According to (4.7), the inviscid growth rate of PSI is independent of the disturbance wavenumber κ so there is no preferred wavelength of instability. Viscous effects stabilize the relatively short waves with $\kappa > \sqrt{\gamma/2\alpha}$, and the maximum growth rate is then obtained for $\kappa = 0$. (Strictly, the asymptotic theory, which assumes fine-scale disturbances obeying (2.14), breaks down for $\kappa \ll 1$; under the present weakly nonlinear nearly inviscid flow conditions, the maximum growth rate is realized for finite but small κ, as illustrated in figure 3 of Koudella & Staquet (2006) and in figure 11(*a*) of Bourget *et al.* (2013).)

The conclusion that the strongest PSI arises for perturbations with small κ, holds only for sinusoidal wavetrains, which have infinite extent ($D \to \infty$). As remarked earlier, in the case of beams with locally confined profile, the duration of the interaction of perturbations with the underlying wave is controlled by the group velocity c/κ, making instability less likely as κ is decreased; as a result, a low-wavenumber cutoff is to be expected, in addition to the high-wavenumber cutoff imposed by viscous effects. Thus, instability, if present at all, occurs in an interval of finite κ, and the maximum growth rate is realized at a certain $\kappa = O(1)$ within this window. A detailed discussion of this scenario follows.

4.2. *Eigenvalue problem*

The stability of beams with locally confined envelope, $\overline{q}(\xi) \to 0$ as $\xi \to \pm\infty$, hinges upon finding normal-mode solutions of (4.4)

$$(a, b^*) = \left(\hat{a}(\xi), \hat{b}^*(\xi)\right) \mathrm{e}^{\lambda\tau}, \tag{4.8}$$

with $\lambda = \lambda_r + \mathrm{i}\lambda_i$, that decay to zero far from the beam:

$$\hat{a} \to 0, \ \hat{b}^* \to 0 \quad (\xi \to \pm\infty)\,. \tag{4.9a,b}$$

Substituting (4.8) into (4.4), $\hat{a}$ and $\hat{b}^*$ thus satisfy

$$\hat{a}_\xi + \hat{\lambda}\hat{a} - \hat{\kappa}\overline{q}\hat{b}^* = 0, \tag{4.10a}$$

$$\hat{b}^*_\xi - \hat{\lambda}\hat{b}^* + \hat{\kappa}\overline{q}^*\hat{a} = 0, \tag{4.10b}$$

with

$$\hat{\lambda} = \left(\lambda + \alpha\kappa^2\right)\frac{D}{c}\kappa, \quad \hat{\kappa} = \frac{\gamma D}{c}\kappa. \tag{4.11a,b}$$

For given envelope profile $\overline{q}(\xi)$, (4.10) along with the boundary conditions (4.9) define an eigenvalue problem, with $\hat{\lambda} = \hat{\lambda}_r + \mathrm{i}\hat{\lambda}_i$ being the eigenvalue and $\hat{\kappa}$ a parameter that controls the perturbation wavenumber κ. Solving this eigenvalue problem provides $\hat{\lambda} = \hat{\lambda}(\hat{\kappa})$, and the stability of the underlying beam is decided by the disturbance growth rate λ_r which follows from (4.11),

$$\lambda_r = \gamma \frac{\hat{\lambda}_r}{\hat{\kappa}} - \frac{\alpha c^2}{D^2 \gamma^2} \hat{\kappa}^2, \tag{4.12}$$

with $\lambda_r > 0$ implying instability.

It is easy to verify that, for given $\overline{q}(\xi)$ and $\hat{\kappa}$, if $\{\hat{\lambda};\ \hat{a},\ \hat{b}^*\}$ is an eigensolution of the problem (4.9) and (4.10), so is $\{-\hat{\lambda}^*;\ \hat{b},\ -\hat{a}^*\}$. Choosing then the mode with $\hat{\lambda}_r > 0$, the first term in (4.12), which derives from the interaction of the disturbance with the beam, is destabilizing, whereas the second term accounts for viscous effects and is stabilizing; the stability of an eigensolution thus depends upon which of these terms prevails. Based on this criterion, a comprehensive stability analysis of a beam with certain envelope $\overline{q}(\xi)$ can be carried out by tracing eigensolution branches as $\hat{\kappa}$ is varied.

In the following, for simplicity, the envelope profile $\overline{q}(\xi)$ will be taken to be real. In this instance, it can readily be shown (see appendix B) that a countable infinity of real eigenvalue branches $\hat{\lambda} = \hat{\lambda}^{(n)}(\hat{\kappa})$ bifurcate at certain critical values of $\hat{\kappa}$:

$$\hat{\kappa}_c^{(n)} = \frac{(2n+1)\pi}{2\displaystyle\int_{-\infty}^{\infty} \overline{q}(\xi)\,\mathrm{d}\xi} \quad (n = 0, 1, 2, \ldots). \tag{4.13}$$

In view of (4.11) and (4.12), the lowest of the bifurcation points (4.13), $\hat{\kappa}_c^{(0)}$, provides a minimum value of the perturbation wavenumber,

$$\kappa_{min} = \frac{c}{\gamma D} \hat{\kappa}_c^{(0)}, \tag{4.14}$$

below which no instability is possible, even in the absence of viscous dissipation. Clearly, this low-wavenumber cutoff for instability is a characteristic only of beams with locally confined profile. As expected, decreasing the beam width D increases κ_{min}, which makes instability less likely. The presence of κ_{min}, combined with the high-wavenumber cutoff due to viscous effects in (4.12), confirms that PSI of a localized beam, if possible at all, is limited to values of κ within a finite window which shrinks as the beam is made narrower.

5. Top-hat beam envelope

As a simple example, we now work out the details of PSI for the top-hat envelope profile

$$\overline{q}(\xi) = \begin{cases} 1/2 & (|\xi| \leqslant 1/2) \\ 0 & (|\xi| > 1/2), \end{cases} \tag{5.1}$$

which represents a uniform sinusoidal wave of peak amplitude ϵ and finite width, similar to the type of beams studied in the laboratory experiments of Bourget *et al.* (2013). For this choice of $\overline{q}(\xi)$, it is feasible to solve the eigenvalue problem (4.9) and (4.10) by analytical means.

Briefly, under the normalization $\hat{a} = \exp(-\hat{\lambda}\xi)$ for $\xi > 1/2$, the appropriate solution of (4.10) that also satisfies conditions (4.9) takes the form

$$\hat{a} = \mathrm{e}^{-\hat{\lambda}\xi}, \quad \hat{b}^* = 0 \quad (\xi > 1/2), \tag{5.2a}$$

$$\hat{a} = 0, \quad \hat{b}^* = \mathbb{D}\mathrm{e}^{\hat{\lambda}\xi} \quad (\xi < -1/2), \tag{5.2b}$$

$$\begin{Bmatrix} \hat{a} \\ \hat{b}^* \end{Bmatrix} = \mathbb{D}_+ \begin{Bmatrix} 1 \\ B_+ \end{Bmatrix} \mathrm{e}^{\mathrm{i}\sigma\xi} + \mathbb{D}_- \begin{Bmatrix} 1 \\ B_- \end{Bmatrix} \mathrm{e}^{-\mathrm{i}\sigma\xi} \quad (|\xi| < 1/2)\,, \tag{5.3}$$

where

$$\sigma = \left(\frac{1}{4}\hat{\kappa}^2 - \hat{\lambda}^2\right)^{1/2}, \quad B_\pm = \frac{2}{\hat{\kappa}}\left(\hat{\lambda} \pm \mathrm{i}\sigma\right), \tag{5.4a,b}$$

and $\mathbb{D}_+$, $\mathbb{D}_-$ and $\mathbb{D}$ are constants to be determined. Enforcing continuity of $\hat{a}$ and $\hat{b}^*$ at $\xi = \pm 1/2$ then leads to the characteristic equation

$$\hat{\lambda}\sin\sigma + \sigma\cos\sigma = 0 \tag{5.5}$$

for the eigenvalues $\hat{\lambda} = \hat{\lambda}(\hat{\kappa})$.

From (5.5), one may verify that a countable infinity of real eigenvalue branches, $\hat{\lambda} = \hat{\lambda}^{(n)}(\hat{\kappa})$, bifurcate at

$$\hat{\kappa}_c^{(n)} = (2n+1)\pi \quad (n = 0, 1, 2, \ldots), \tag{5.6}$$

in agreement with (4.13). On each of these solution branches and $\hat{\kappa}$ slightly above the bifurcation point $\hat{\kappa}_c^{(n)}$,

$$\hat{\lambda}^{(n)} = \frac{(2n+1)\pi}{4}\left(\hat{\kappa} - \hat{\kappa}_c^{(n)}\right) + \cdots, \tag{5.7}$$

while, in the other extreme, $\hat{\kappa} \gg \hat{\kappa}_c^{(n)}$,

$$\hat{\lambda}^{(n)} \sim \frac{1}{2}\hat{\kappa} - \frac{n^2\pi^2}{\hat{\kappa}} + \cdots. \tag{5.8}$$

In view of (4.11) and (4.12), the leading-order term in (5.8) recovers the growth rate (4.7) of PSI for a uniform sinusoidal wave; as expected, for very short subharmonic disturbances ($\kappa \gg 1$), a nearly monochromatic localized beam behaves like an infinite sinusoidal wavetrain. Moreover, the same is true when the width of the beam envelope is increased ($D \gg 1$) for $\kappa = O(1)$ fixed, since $\hat{\kappa} \gg 1$ in this limit as well, according to (4.11).

Returning now to expression (4.12) for the disturbance growth rate λ_r, instability ($\lambda_r > 0$) arises if

$$\hat{\lambda}(\hat{\kappa}) > \mathbb{C}\hat{\kappa}^3, \tag{5.9}$$

where

$$\mathbb{C} = \frac{\alpha c^2}{\gamma^3 D^2}. \tag{5.10}$$

Figure 3 shows the first three eigensolution branches $\hat{\lambda} = \hat{\lambda}^{(n)}(\hat{\kappa})$ of the characteristic equation (5.5), which bifurcate at $\hat{\kappa}_c^{(n)} = (2n+1)\pi$ ($n = 0, 1, 2$) according to (5.6), along with the cubic in $\hat{\kappa}$ on the right-hand side of (5.9), taking $\mathbb{C} = 1.5 \times 10^{-3}$ for

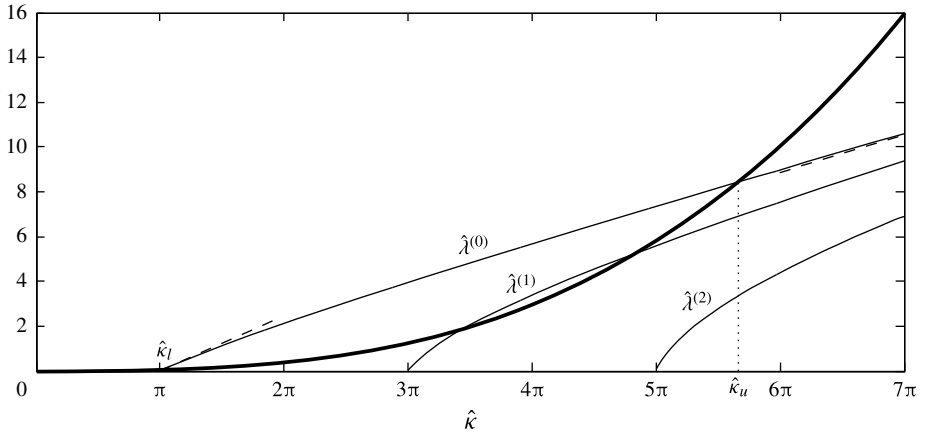

FIGURE 3. Plots (—) of the first three eigenvalue branches $\hat{\lambda}^{(n)}(\hat{\kappa})$ of the characteristic equation (5.5), which bifurcate at $\hat{\kappa}_c^{(n)} = (2n+1)\pi$ for $n = 0, 1, 2$. The intersections of the lowest ($n = 0$) of these modes with the cubic $\mathbb{C}\hat{\kappa}^3$ (—), shown here for $\mathbb{C} = 1.5 \times 10^{-3}$, determine the range of unstable disturbance wavenumbers $\hat{\kappa}_l < \hat{\kappa} < \hat{\kappa}_u$. The dashed lines (– –) indicate the asymptotic approximations (5.7) and (5.8) of $\hat{\lambda}^{(0)}(\hat{\kappa})$ near and far away from the bifurcation point $\hat{\kappa}_c^{(0)}$, respectively.

illustration. For this $\mathbb{C}$, the cubic intersects the first two eigensolution branches ($n = 0, 1$), so for a certain range of $\hat{\kappa}$ the instability condition (5.9) can be satisfied by either of these modes; however, the lowest mode ($n = 0$) always provides the dominant instability (largest growth rate) since $\hat{\lambda}^{(0)}(\hat{\kappa}) > \hat{\lambda}^{(1)}(\hat{\kappa})$. Specifically, there is a finite range of unstable disturbance wavenumbers, $\hat{\kappa}_l < \hat{\kappa} < \hat{\kappa}_u$, where $\hat{\kappa}_l$ and $\hat{\kappa}_u$ denote the values of $\hat{\kappa}$ at which the cubic $\mathbb{C}\hat{\kappa}^3$ intersects the lowest-eigenvalue curve (figure 3). Within this finite window of instability, the wavenumber that has the maximum growth rate (4.12) is expected to emerge from a general initial perturbation as the preferred scale of PSI.

It is clear from figure 3 that, in order for the cubic $\mathbb{C}\hat{\kappa}^3$ to intersect the eigenvalue curve $\hat{\lambda}^{(0)}(\hat{\kappa})$, and hence instability to be possible, the parameter $\mathbb{C}$ in (5.10) must be less than a critical value $\mathbb{C}_c$ ($= 0.0108$),

$$\mathbb{C} < \mathbb{C}_c. \tag{5.11}$$

Combining (5.10) with (2.15), this condition for instability can be written as

$$\frac{\epsilon}{\nu^{1/2}} \frac{\gamma^{3/2}}{c} D > \left(\frac{1}{2\mathbb{C}_c}\right)^{1/2}. \tag{5.12}$$

Thus, PSI of a locally confined beam is controlled by: $\epsilon/\nu^{1/2}$, the strength of nonlinear relative to viscous effects; the beam frequency which fixes the beam propagation direction and hence c and γ according to (2.13) and (4.5); and D, which fixes the envelope width. More specifically, for given Reynolds number $1/\nu$, a beam of certain frequency and amplitude parameter ϵ becomes unstable when D exceeds the critical value

$$D_c = \left(\frac{1}{2\mathbb{C}_c}\right)^{1/2} \frac{c}{\gamma^{3/2}} \frac{\nu^{1/2}}{\epsilon}. \tag{5.13}$$

Recalling the scaling (4.2), the critical envelope width D_c translates into a minimum number of carrier wavelengths,

$$N_c = \frac{1}{2\pi}\left(\frac{1}{2\mathbb{C}_c}\right)^{1/2}\frac{c}{\gamma^{3/2}}\frac{\nu^{1/2}}{\epsilon^{3/2}}, \tag{5.14}$$

which a weakly nonlinear nearly monochromatic beam must comprise to develop PSI. Note that, since $\nu^{1/2}/\epsilon = O(1)$ according to (2.15), $N_c = O(\epsilon^{-1/2})$.

Although it was derived for the particular envelope profile (5.1), the instability condition (5.12) holds in general for real, locally confined envelopes, as suggested by the bifurcation analysis of the eigenvalue problem (4.9) and (4.10) presented in appendix B; only the value of $\mathbb{C}_c$ depends on the specific envelope shape. Hence, the stability criterion (5.12) as well as expressions (5.13) and (5.14) for the minimum envelope width and number of cycles, respectively, required for instability, are also generally valid.

6. Transient disturbance evolution

We now turn attention to the long-time evolution of PSI, when unstable disturbances are no longer infinitesimal and full coupling with the underlying beam is in effect, as described by (3.9) and (3.10).

As in the simulations of Clark & Sutherland (2010), here the unperturbed beam is taken to have a Gaussian envelope profile, in the normalized form

$$\overline{q}(\xi) = \tfrac{1}{2}\exp\left(-\xi^2\right), \tag{6.1}$$

so that the wave streamfunction has peak amplitude ϵ. The assumed initial perturbations consist of small subharmonic disturbances that are locally confined in the beam vicinity and whose wavenumber κ is within the window of instability predicted by the linear stability analysis of § 4.2.

For the envelope profile (6.1), in particular, it follows from the eigenvalue problem (4.9) and (4.10) that the fundamental eigensolution branch $\hat{\lambda}^{(0)}(\hat{\kappa})$, which bifurcates at $\hat{\kappa}_c^{(0)} = \sqrt{\pi}$ according to (4.13), intersects with the cubic $\mathbb{C}\hat{\kappa}^3$ when $\mathbb{C} < \mathbb{C}_c = 2.66 \times 10^{-2}$. (The eigenvalues were computed numerically, solving (4.9) and (4.10) by centred finite differences on a uniform grid with $\Delta\xi = 0.01$ and $-10 < \xi < 10$.) Taking $\mathbb{C} = 5 \times 10^{-3}$, instability then arises for $1.81 < \hat{\kappa} < 9.15$. In addition, we choose $D = 1$ for the envelope width and $\theta = \pi/4$ for the beam propagation angle to the horizontal; this, in turn, fixes the beam frequency $\omega = \sin\theta = 1/\sqrt{2}$, the subharmonic propagation angle $\phi = \sin^{-1}(\omega/2) = 0.3614$, the group velocity $c = 0.3849$ in (2.13), the parameter $\gamma = 0.3932$ in (4.5), and $\alpha = 2.05 \times 10^{-3}$ in view of (5.10). Thus, from (4.11), the disturbance wavenumber $\kappa = 0.9788\hat{\kappa}$, so the range of unstable wavenumbers is $1.77 < \kappa < 8.96$, with the largest growth rate (4.12) corresponding to $\kappa = 4.29$.

The evolution equations (3.9) and (3.10) were solved numerically using as initial conditions

$$q = \overline{q}(\xi), \quad a = b = \frac{\overline{q}(\xi)}{100} \quad (\tau = 0), \tag{6.2a–c}$$

with $\overline{q}(\xi)$ given by (6.1), and perturbation wavenumber within the unstable range $1.77 < \kappa < 8.96$ determined above. The numerical method used second-order centred finite differences on a uniform grid, with $\Delta\xi = 0.02$ and $-25 < \xi < 25$, and fourth-order Runge–Kutta time stepping with $\Delta t = 0.005$.

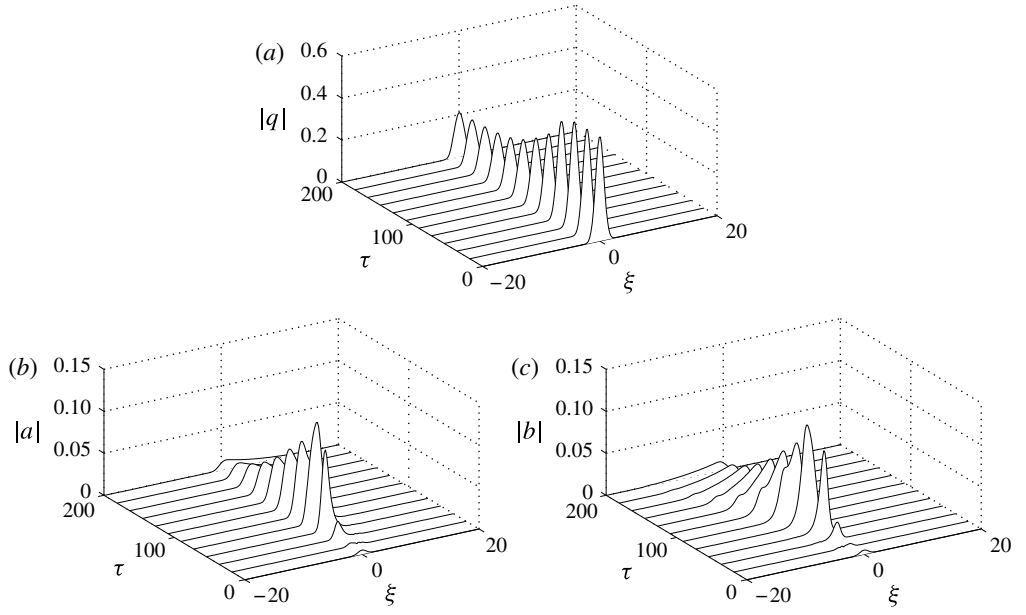

FIGURE 4. Evolution of wave beam, with initially Gaussian envelope (6.1), and subharmonic perturbations with the most unstable wavenumber, according to numerical solution of the coupled equations (3.9) and (3.10) subject to the initial conditions (6.2). The wave envelope magnitudes of the beam ($|q|$) and the perturbations ($|a|$, $|b|$) are displayed at various times τ.

As the initial perturbations in (6.2) are small relative to the uniform beam, in the early stages of our computations the disturbance evolution is governed by the linearized system (4.4), confirming the predictions of the linear stability analysis. After an initial adjustment period, a and b adapt to the fundamental instability eigenmode and grow exponentially in τ with the growth rate (4.12) corresponding to the chosen value of κ. However, since a and b grow at the expense of q according to the fully coupled equation system (3.9) and (3.10), this exponential growth cannot be sustained: as the beam becomes less steep, the subharmonic wavepackets can no longer stay locked onto it; as a result, the nonlinear wave interaction comes to an end, and the linearly unstable disturbances eventually decay due to viscous dissipation as they move away from the beam with their respective group velocities.

This scenario is illustrated in figure 4 for subharmonic perturbations with the most unstable wavenumber, $\kappa = 4.29$. Note that the maximum combined amplitude of these disturbances, reached at $\tau \approx 64$, is comparable to the beam peak amplitude at that time, and the final beam peak amplitude, after the perturbations have died out, is roughly 40 % of its initial value. Hence, the stability parameter $\mathbb{C}$, which is inversely proportional to the square of the beam amplitude ϵ according to (2.15) and (5.10), has effectively been increased by roughly a factor of 6, so finally $\mathbb{C} \approx 3 \times 10^{-2}$; as this exceeds the critical value for instability, $\mathbb{C}_c = 2.66 \times 10^{-2}$, the final beam profile is thus stable according to (5.11).

These findings indicate that the overall effect of PSI in the weakly nonlinear regime is transfer of energy to short-scale subharmonic perturbations, which ultimately decay by viscous dissipation, leaving behind a stable beam. However, the rapid growth of these perturbations and the fact that they become as strong as the underlying beam,

suggest that overturning and/or shear instability leading to breakdown may be possible due to PSI, in the case of beams with $O(1)$ non-dimensional amplitude. These finite-amplitude phenomena, of course, are beyond the reach of the present weakly nonlinear theory.

7. Concluding remarks

As revealed by the preceding analysis, in order for PSI of locally confined internal wave beams to set in, subharmonic perturbations must overlap with the underlying beam for long enough time to allow triad interactions to act. Specifically, for a beam with amplitude parameter $\epsilon \ll 1$, the time required for triad interactions to come into play is $O(1/\epsilon)$. In the case of localized beams with general profile of $O(1)$ width, according to the evolution equations (2.18), this nonlinear interaction time scale is longer than $t = O(\epsilon^{-1/2})$, the time it takes short-scale subharmonic wavepackets to travel across the beam. As a result, no PSI is possible save for the resonant situation where the wavepacket group velocity happens to vanish or nearly so.

On the other hand, when the beam profile is nearly monochromatic, comprising a sinusoidal carrier with $O(1)$ wavelength modulated by a locally confined envelope of $O(\epsilon^{-1/2})$ width, short-scale subharmonic perturbations evolve on the same time scale, $t = O(1/\epsilon)$, as triad interactions. Thus, the propagation of subharmonic disturbances is in balance with nonlinear-interaction effects and weak viscous dissipation, as indicated by the evolution equations (3.8) and (3.9). In this instance, if the beam obeys condition (5.12), PSI is possible for a finite range of disturbance wavenumbers.

According to the stability criterion (5.12), larger-amplitude and wider beams are more prone to PSI. Specifically, given the fluid stratification and viscosity, a beam of certain carrier wavelength and small amplitude can suffer PSI if its width exceeds the threshold (5.13); thus, the beam profile must comprise a minimum number of carrier wavelengths for instability to arise. In keeping with our assumption of weakly nonlinear nearly monochromatic beams, this critical number turns out to be relatively large, $N_c = O(\epsilon^{-1/2})$. The theoretical stability criterion (5.12) could be confirmed by numerical simulations and perhaps laboratory experiments. In fact, in very recent experimental and numerical work, Bourget *et al.* (2014) have confirmed that the finite width of a beam does play an important role in resonant-triad instability; however, as in their earlier study (Bourget *et al.* 2013), owing to viscous effects, the unstable perturbations were not of the short-scale subharmonic type discussed here.

The conclusion reached here, that nearly monochromatic wave beams can suffer PSI as opposed to localized beams of $O(1)$ width which were found to be stable, seems consistent with the experiments and simulations of Clark & Sutherland (2010). As noted in § 1, a novel feature of these experiments was that wave beams were induced via a cylinder performing relatively large-amplitude vertical oscillations (amplitude-to-diameter ratio $\approx$0.33). In response to this forcing, the turbulent oscillatory flow surrounding the cylinder acted as wave source, and the resulting quasi-monochromatic wave beams were observed to breakdown due to PSI. By contrast, no PSI was detected in relatively thin beams generated by similar means, but with a cylinder performing smaller-amplitude oscillations (amplitude-to-diameter ratio $\approx$0.10), in which case the beam width was set by the cylinder radius (Sutherland *et al.* 1999; Sutherland & Linden 2002).

Quantitative comparison of the predictions of the asymptotic analysis with Clark & Sutherland (2010), strictly, is not feasible since the experimentally observed beams, as well as those used as initial conditions in companion simulations, had finite

amplitude and involved only roughly two carrier wavelengths. Specifically, using $L_* = 1/k_\sigma$, where $k_\sigma \approx 0.6$ cm^{-1} is the experimentally observed carrier wavenumber, the wave amplitude parameter ϵ defined in (2.5) of the beam used in these simulations, is estimated from figure 15(*a*) of Clark & Sutherland (2010) as $\epsilon = 0.79, 0.55$ for the stratified solution of NaCl and NaI, respectively. To convert the Gaussian envelope profile used in their simulations to the normalized form (6.1), the dimensionless width parameter $D = \sqrt{2}\epsilon^{1/2}k_\sigma\sigma_0$, where σ_0 is the (dimensional) standard deviation. Taking σ_0 as a quarter of the beam width, $k_\sigma\sigma_0 \approx 2.6$ according to figure 15(*a*), which translates into $4\sigma_0(k_\sigma/2\pi) \approx 1.65$ carrier wavelengths contained in the beam; also, $D \approx 3.2, 2.7$ for the solution of NaCl and NaI, respectively.

For these ϵ, D and $\theta = \pi/4$ for the beam propagation angle, the values of the stability parameter in (5.10) for the two stratified solutions turn out to be $\mathbb{C} \approx (3.2, 6.4) \times 10^{-4}$, well below the critical value $\mathbb{C}_c = 2.66 \times 10^{-2}$ for the Gaussian (6.1). Hence, the beam profile in the simulations is clearly unstable according to the linear stability criterion (5.11). Moreover, from (4.12), the theoretical maximum instability growth rate, $\epsilon N_0 \lambda_r|_{max} \approx 0.2$ s^{-1}, is about twice the numerical growth rate estimated from figure 15(*b*,*c*) of Clark & Sutherland (2010). Also, the theoretically most unstable wavelength over predicts by a factor of approximately two the preferred instability wavelength found in the simulations. Given that the beam used as initial condition in the simulations did not actually have small amplitude and slowly modulated profile, this rough quantitative agreement with the asymptotic analysis seems reasonable.

Acknowledgement

This work was supported in part by the US National Science Foundation under grant DMS-1107335.

Appendix A. Derivation of wave-interaction equations

Here, we provide some intermediate steps in the derivation of the evolution equations (2.11) and (2.12). Interactions between the underlying beam and subharmonic perturbations appear through nonlinear resonant terms and are best organized by phase,

$$\begin{aligned} \mathrm{J}(\rho, \psi) \;=\; & \mu\delta^2 \left\{\mathrm{J}(F\mathrm{e}^{\mathrm{i}\zeta/\mu}, B\mathrm{e}^{-\mathrm{i}\zeta/\mu}) + \mathrm{J}(G\mathrm{e}^{-\mathrm{i}\zeta/\mu}, A\mathrm{e}^{\mathrm{i}\zeta/\mu})\right\} \mathrm{e}^{-\mathrm{i}\omega t} \\ & + \epsilon\delta \left\{\mathrm{J}(G^*\mathrm{e}^{\mathrm{i}\zeta/\mu}, Q) + \mu\mathrm{J}(R, B^*\mathrm{e}^{\mathrm{i}\zeta/\mu})\right\} \mathrm{e}^{-\mathrm{i}\omega t/2} \\ & + \epsilon\delta \left\{\mathrm{J}(F^*\mathrm{e}^{-\mathrm{i}\zeta/\mu}, Q) + \mu\mathrm{J}(R, A^*\mathrm{e}^{-\mathrm{i}\zeta/\mu})\right\} \mathrm{e}^{-\mathrm{i}\omega t/2} + \text{c.c.}, \qquad \text{(A 1)} \\ \mathrm{J}(\nabla^2\psi, \psi) \;=\; & (\mu\delta)^2 \left\{\mathrm{J}(\mathbb{A}\mathrm{e}^{\mathrm{i}\zeta/\mu}, B\mathrm{e}^{-\mathrm{i}\zeta/\mu}) + \mathrm{J}(\mathbb{B}\mathrm{e}^{-\mathrm{i}\zeta/\mu}, A\mathrm{e}^{\mathrm{i}\zeta/\mu})\right\} \mathrm{e}^{-\mathrm{i}\omega t} \\ & + \mu\epsilon\delta \left\{\mathrm{J}(Q_{\eta\eta}, B^*\mathrm{e}^{\mathrm{i}\zeta/\mu}) + \mathrm{J}(\mathbb{B}^*\mathrm{e}^{\mathrm{i}\zeta/\mu}, Q)\right\} \mathrm{e}^{-\mathrm{i}\omega t/2} \\ & + \mu\epsilon\delta \left\{\mathrm{J}(Q_{\eta\eta}, A^*\mathrm{e}^{-\mathrm{i}\zeta/\mu}) + \mathrm{J}(\mathbb{A}^*\mathrm{e}^{-\mathrm{i}\zeta/\mu}, Q)\right\} \mathrm{e}^{-\mathrm{i}\omega t/2} + \text{c.c.}, \qquad \text{(A 2)} \end{aligned}$$

where

$$\mathbb{A}\mathrm{e}^{\mathrm{i}\zeta/\mu} \;\equiv\; \nabla^2 A\mathrm{e}^{\mathrm{i}\zeta/\mu} = \left\{\frac{-1}{\mu^2}A + 2\frac{\mathrm{i}}{\mu}\cos\chi A_\eta + A_{\eta\eta}\right\} \mathrm{e}^{\mathrm{i}\zeta/\mu}, \qquad \text{(A 3)}$$

$$\mathbb{B}\mathrm{e}^{-\mathrm{i}\zeta/\mu} \;\equiv\; \nabla^2 B\mathrm{e}^{-\mathrm{i}\zeta/\mu} = \left\{\frac{-1}{\mu^2}B - 2\frac{\mathrm{i}}{\mu}\cos\chi B_\eta + B_{\eta\eta}\right\} \mathrm{e}^{-\mathrm{i}\zeta/\mu}, \qquad \text{(A 4)}$$

and $\chi = \theta - \phi$.

The evolution equation (2.11) for Q is derived by substituting expansions (2.10) in the governing equations (2.1) and (2.2) and collecting terms proportional to $\exp(-\mathrm{i}\omega t)$. Making use of the first set of curly brackets in (A 1), it follows from (2.1) that

$$R = -\mathrm{i}Q_\eta - \mu\frac{1}{\omega}Q_{\eta T} + \mu^2\frac{\mathrm{i}}{\omega^2}Q_{\eta TT} + \frac{\delta^2}{\epsilon}\frac{\sin\chi}{\omega}\,(AG - BF)_\eta + O\left(\mu^3, \mu\delta^2/\epsilon\right). \tag{A 5}$$

Upon substituting (A 5) in (2.2) and using (A 2), one then has

$$\left\{\mu Q_T - \frac{\mathrm{i}}{2\omega}\mu^2 Q_{TT} + \frac{\delta^2}{2\epsilon}\sin\chi\,(2\cos\chi AB + BF - AG) - \frac{\nu}{2}Q_{\eta\eta}\right\}_{\eta\eta} = O(\mu^3, \mu\delta^2/\epsilon). \tag{A 6}$$

Next, to derive the evolution equations (2.12), we collect terms proportional to $\exp(\pm\mathrm{i}\zeta/\mu - \mathrm{i}\omega t/2)$. Specifically, making use of (A 1), it follows from (2.1) that

$$\begin{aligned} F \;=\; & A - 2\mathrm{i}\mu\left(\frac{1}{\omega}A_T + A_\eta\right) - \frac{4\mu^2}{\omega}\left(\frac{1}{\omega}A_{TT} + A_{\eta T}\right) - \frac{2\epsilon}{\mu}\frac{\sin\chi}{\omega}Q_\eta G^* \\ & + 4\mathrm{i}\epsilon\frac{\sin\chi}{\omega^2}\left(Q_\eta G^*\right)_T - 2\mathrm{i}\epsilon\frac{\sin\chi}{\omega}Q_{\eta\eta}B^* + O(\mu^3, \epsilon\mu, \delta^2), \end{aligned} \tag{A 7}$$

$$\begin{aligned} G \;=\; & -B + 2\mathrm{i}\mu\left(\frac{1}{\omega}B_T - B_\eta\right) + \frac{4\mu^2}{\omega}\left(\frac{1}{\omega}B_{TT} - B_{\eta T}\right) + \frac{2\epsilon}{\mu}\frac{\sin\chi}{\omega}Q_\eta F^* \\ & - 4\mathrm{i}\epsilon\frac{\sin\chi}{\omega^2}(Q_\eta F^*)_T + 2\mathrm{i}\epsilon\frac{\sin\chi}{\omega}Q_{\eta\eta}A^* + O(\mu^3, \epsilon\mu, \delta^2). \end{aligned} \tag{A 8}$$

Also, making use of (A 2), it follows from (2.2) that

$$\begin{aligned} A \;=\; & F - 2\mathrm{i}\mu\left\{\frac{1}{\omega}A_T - \cos\chi A_\eta + F_\eta\right\} + \mu^2\left\{A_{\eta\eta} - \frac{4\cos\chi}{\omega}A_{\eta T}\right\} - \mathrm{i}\frac{2\nu}{\omega\mu^2}A \\ & - \frac{\epsilon}{\mu}\frac{2\sin\chi}{\omega}Q_\eta B^* - \mathrm{i}\epsilon\frac{2\sin 2\chi}{\omega}Q_\eta B^*_\eta + O(\epsilon\mu, \mu^3), \end{aligned} \tag{A 9}$$

$$\begin{aligned} B \;=\; & -G - 2\mathrm{i}\mu\left\{\frac{1}{\omega}B_T + \cos\chi B_\eta + G_\eta\right\} + \mu^2\left\{B_{\eta\eta} + \frac{4\cos\chi}{\omega}B_{\eta T}\right\} - \mathrm{i}\frac{2\nu}{\omega\mu^2}B \\ & + \frac{\epsilon}{\mu}\frac{2\sin\chi}{\omega}Q_\eta A^* + \mathrm{i}\epsilon\frac{2\sin 2\chi}{\omega}Q_\eta A^*_\eta + O(\epsilon\mu, \mu^3). \end{aligned} \tag{A 10}$$

Putting the leading order balance, $F = A$ and $G = -B$, from the above into (A 6) produces (2.11).

Using (A 7) and (A 8) to eliminate F and G from (A 9) and (A 10), we obtain

$$\begin{aligned} & \mu\left\{A_T + \frac{\omega}{2}(2 - \cos\chi)A_\eta\right\} - \mathrm{i}\mu^2\left\{\frac{3\omega}{4}A_{\eta\eta} + (2 + \cos\chi)\,A_{\eta T} + \frac{1}{\omega}A_{TT}\right\} + \frac{\nu}{2\mu^2}A \\ & \quad + \epsilon\sin\chi\left\{\frac{3}{2}Q_{\eta\eta}B^* + (2 - \cos\chi)\,Q_\eta B^*_\eta + \frac{1}{\omega}Q_{\eta T}B^*\right\} - \mathrm{i}\frac{\epsilon^2}{\mu^2}\frac{\sin^2\chi}{\omega}\left|Q_\eta\right|^2 A \\ & = O\left(\mu^3, \epsilon\mu, \delta^2, \epsilon^2/\mu\right), \end{aligned} \tag{A 11}$$

$$\mu\left\{B_T-\frac{\omega}{2}\left(2-\cos\chi\right)B_\eta\right\}-\mathrm{i}\mu^2\left\{\frac{3\omega}{4}B_{\eta\eta}-\left(2+\cos\chi\right)B_{\eta T}+\frac{1}{\omega}B_{TT}\right\}+\frac{\nu}{2\mu^2}B$$
$$+\epsilon\sin\chi\left\{\frac{3}{2}Q_{\eta\eta}A^*+\left(2-\cos\chi\right)Q_\eta A^*_\eta-\frac{1}{\omega}Q_{\eta T}A^*\right\}-\mathrm{i}\frac{\epsilon^2}{\mu^2}\frac{\sin^2\chi}{\omega}\left|Q_\eta\right|^2B$$
$$=O\left(\mu^3,\epsilon\mu,\delta^2,\epsilon^2/\mu\right). \tag{A 12}$$

Finally, to obtain the evolution equations (2.12) for the subharmonic envelopes A and B, we eliminate $A_{\eta T}, A_{TT}, B_{\eta T}$ and B_{TT} in favour of $A_{\eta\eta}$ and $B_{\eta\eta}$ by using the leading-order balance in (A 11) and (A 12).

Appendix B. Bifurcation of eigensolution branches

Here we show that, for real beam envelope $\overline{q}(\xi)$, the stability eigenvalue problem (4.9) and (4.10) admits a countable infinity of real eigenvalue branches, $\hat\lambda=\hat\lambda^{(n)}(\hat\kappa)$, which bifurcate at certain critical values of the wavenumber parameter, $\hat\kappa=\hat\kappa_c^{(n)}$ $(n=0,1,2,\ldots)$.

In the vicinity of each bifurcation point, where $0<\hat\lambda\ll1$, we expand

$$\hat a=\hat a_0+\hat\lambda\hat a_1+\cdots,\quad \hat b^*=\hat b_0^*+\hat\lambda\hat b_1^*+\cdots, \tag{B 1a}$$

with

$$\hat\kappa=\hat\kappa_c^{(n)}+\hat\lambda\hat\kappa_1^{(n)}+\cdots. \tag{B 1b}$$

Since $\overline{q}(\xi)\to0$ $(\xi\to\pm\infty)$, the far-field (outer) solution of (4.9) and (4.10) is taken in the form

$$\hat a=\mathrm{e}^{-\tilde\xi},\quad \hat b^*=0\quad(\tilde\xi>0), \tag{B 2a}$$
$$\hat a=0,\quad \hat b^*=K\mathrm{e}^{\tilde\xi}\quad(\tilde\xi<0), \tag{B 2b}$$

where $\tilde\xi=\hat\lambda\xi$ and K is a constant to be specified by matching with the near-field (inner) solution, valid for $\xi=O(1)$. Specifically, upon substituting (B 1) in (4.10), $\hat a_0$ and $\hat b_0$ satisfy

$$\hat a_{0\xi}-\hat\kappa_c^{(n)}\overline{q}\hat b_0^*=0, \tag{B 3a}$$
$$\hat b_{0\xi}^*+\hat\kappa_c^{(n)}\overline{q}\hat a_0=0, \tag{B 3b}$$

from which it follows that $\hat a_0^2+\hat b_0^{*2}$ is independent of ξ. Thus, to be consistent with the inner limit (as $\tilde\xi\to0$) of the outer solution (B 2), we set $\hat a_0^2+\hat b_0^{*2}=1$ so $K=\pm1$ in (B 2*b*), and the appropriate matching conditions for $\hat a_0$ and $\hat b_0^*$ are

$$\hat a_0\to1,\quad \hat b_0^*\to0\quad(\xi\to\infty), \tag{B 4a}$$
$$\hat a_0\to0,\quad \hat b_0^*\to\pm1\quad(\xi\to-\infty). \tag{B 4b}$$

Equations (B 3), subject to (B 4), admit a countable infinity of eigensolutions

$$\hat a_0^{(n)}=(-1)^n\sin\left\{\hat\kappa_c^{(n)}\int_{-\infty}^{\xi}\overline{q}\left(\xi'\right)\mathrm{d}\xi'\right\}, \tag{B 5a}$$
$$\hat b_0^{*(n)}=(-1)^n\cos\left\{\hat\kappa_c^{(n)}\int_{-\infty}^{\xi}\overline{q}\left(\xi'\right)\mathrm{d}\xi'\right\}, \tag{B 5b}$$

where

$$\hat\kappa_c^{(n)}=\frac{(2n+1)\pi}{2\displaystyle\int_{-\infty}^{\infty}\overline{q}(\xi)\,\mathrm{d}\xi}\quad(n=0,1,2,\ldots) \tag{B 6}$$

are the bifurcation points of the corresponding eigenvalue branches.

REFERENCES

BELL, T. H. 1975 Lee waves in stratified flows with simple harmonic time dependence. *J. Fluid Mech.* **67**, 705–722.

BOURGET, B., DAUXOIS, T., JOUBAND, S. & ODIER, P. 2013 Experimental study of parametric subharmonic instability for internal plane waves. *J. Fluid Mech.* **723**, 1–20.

BOURGET, B., SCOLAN, H., DAUXOIS, T., LE BARS, M., ODIER, P. & JOUBAUD, S. 2014 Finite-size effects in parametric subharmonic instability. *J. Fluid Mech.* (in press).

CLARK, H. A. & SUTHERLAND, B. R. 2010 Generation, propagation, and breaking of an internal wave beam. *Phys. Fluids* **22**, 076601.

COLE, S. T., RUDNICK, D. L., HODGES, B. A. & MARTIN, J. P. 2009 Observations of tidal internal wave beams at Kauai Channel, Hawaii. *J. Phys. Oceanogr.* **39** (2), 421–436.

GERKEMA, T., STAQUET, C. & BOURUET-AUBERTOT, P. 2006 Decay of semi-diurnal internal-tide beams due to subharmonic resonance. *Geophys. Res. Lett.* **33**, L08604.

GOSTIAUX, L. & DAUXOIS, T. 2007 Laboratory experiments on the generation of internal tidal beams over steep slopes. *Phys. Fluids* **19** (2), 028102.

HIBIYA, T., NAGASAWA, M. & NIWA, Y. 2002 Nonlinear energy transfer within the oceanic internal wave spectrum at mid and high latitudes. *J. Geophys. Res.* **107** (C11), 3207.

JOHNSTON, T. M. S., RUDNICK, D. L., CARTER, G. S., TODD, R. E. & COLE, S. T. 2011 Internal tidal beams and mixing near Monterey Bay. *J. Geophys. Res.* **116**, C03017.

KARIMI, H. H. 2015 Doctoral dissertation. Department of Mechanical Engineering, MIT (in preparation).

KHATIWALA, S. 2003 Generation of internal tides in an ocean of finite depth: analytical and numerical calculations. *Deep-Sea Res.* **50**, 3–21.

KOUDELLA, C. R. & STAQUET, C. 2006 Instability mechanisms of a two-dimensional progressive internal gravity wave. *J. Fluid Mech.* **548**, 165–196.

LAMB, K. G. 2004 Nonlinear interaction among internal wave beams generated by tidal flow over supercritical topography. *Geophys. Res. Lett.* **31**, L09313.

LIEN, R.-C. & GREGG, M. C. 2001 Observations of turbulence in a tidal beam and across a coastal ridge. *J. Geophys. Res.* **106** (C3), 4575–4591.

MACKINNON, J. A., ALFORD, M. H., SUN, O., PINKEL, R., ZHAO, Z. & KLYMAK, J. 2013 Parametric subharmonic instability of the internal tide at 29°N. *J. Phys. Oceanogr.* **43**, 17–28.

MCEWAN, A. D. 1973 Interactions between internal gravity waves and their traumatic effect on a continuous stratification. *Boundary-Layer Meteorol.* **5**, 159–175.

MCEWAN, A. D. & PLUMB, R. A. 1977 Off-resonant amplification of finite internal wave packets. *Dyn. Atmos. Oceans* **2**, 83–105.

MOWBRAY, D. E. & RARITY, B. S. 1967 A theoretical and experimental investigation of the phase configuration of internal waves of small amplitude in a density stratified fluid. *J. Fluid Mech.* **28**, 1–16.

PAIRAUD, I., STAQUET, C., SOMMERIA, J. & MAHDIZADEH, M. 2010 Generation of harmonics and sub-harmonics from an internal tide in a uniformly stratified fluid: numerical and laboratory experiments. In *IUTAM Symposium on Turbulence in the Atmosphere and Oceans* (ed. D. Dritschel), vol. 28, pp. 51–62. Springer.

PEACOCK, T., ECHEVERRI, P. & BALMFORTH, N. J. 2008 An experimental investigation of internal tide generation by two-dimensional topography. *J. Phys. Oceanogr.* **38** (1), 235–242.

PHILLIPS, O. M. 1981 Wave interactions—the evolution of an idea. *J. Fluid Mech.* **106**, 215–227.

STAQUET, C. & SOMMERIA, J. 2002 Internal gravity waves: from instabilities to turbulence. *Annu. Rev. Fluid Mech.* **34**, 559–593.

SUTHERLAND, B. R. 2013 The wave instability pathway to turbulence. *J. Fluid Mech.* **724**, 1–4.

SUTHERLAND, B. R., DALZIEL, S. B., HUGHES, G. O. & LINDEN, P. F. 1999 Visualization and measurement of internal waves by 'synthetic schlieren'. Part 1. Vertically oscillating cylinder. *J. Fluid Mech.* **390**, 93–126.

SUTHERLAND, B. R. & LINDEN, P. F. 2002 Internal wave excitation by a vertically oscillating elliptical cylinder. *Phys. Fluids* **14** (2), 721–731.

TABAEI, A. & AKYLAS, T. R. 2003 Nonlinear internal gravity wave beams. *J. Fluid Mech.* **482**, 141–161.

YOUNG, W. R., TSANG, Y.-K. & BALMFORTH, N. J. 2008 Near-inertial parametric subharmonic instability. *J. Fluid Mech.* **607**, 25–49.

ZHANG, H. P., KING, B. & SWINNEY, H. L. 2007 Experimental study of internal gravity waves generated by supercritical topography. *Phys. Fluids* **19**, 096602.

ZHOU, Q. & DIAMESSIS, P. J. 2013 Reflection of an internal gravity wave beam off a horizontal free-slip surface. *Phys. Fluids* **25**, 036601.